Stability of orientationally disordered crystal structures of colloidal hard dumbbells

Matthieu Marechal and Marjolein Dijkstra
Soft Condensed Matter, Debye Institute for NanoMaterials Science, Utrecht University, Princetonplein 5, 3584 CC Utrecht, The Netherlands

(Received 10 March 2008; published 13 June 2008)

We study the stability of orientationally disordered crystal phases in a suspension of colloidal hard dumbbells using Monte Carlo simulations. For dumbbell bond length $L/\sigma<0.4$ with L the separation of the two spheres of the dumbbell and σ the diameter of the spheres, we determine the difference in Helmholtz free energy of a plastic crystal with a hexagonal-close-packed (hcp) and a face-centered-cubic (fcc) structure using thermodynamic integration and the lattice-switch Monte Carlo method. We find that the plastic crystal with the hcp structure is more stable than the one with the fcc structure for a large part of the stable plastic crystal regime. In addition, we study the stability of an orientationally disordered aperiodic crystal structure in which the spheres of the dumbbells are on a random-hexagonal-close-packed lattice, and the dumbbells are formed by taking random pairs of neighboring spheres. Using free-energy calculations, we determine the fluid-aperiodic crystal and periodic-aperiodic crystal coexistence regions for $L/\sigma>0.88$.

DOI: 10.1103/PhysRevE.77.061405 PACS number(s): 82.70.Dd, 64.70.D−, 81.30.Dz

I. INTRODUCTION

Originally, hard dumbbells were studied as a suitable model for simple nonspherical diatomic or polyatomic molecules, such as nitrogen and carbon dioxide. In particular, the structure and thermodynamics of the fluid phase of hard dumbbells were investigated, since the structure of molecular liquids is mainly determined by excluded volume effects [1]. Additionally, in order to understand the stable crystal structures in molecular systems, the solid-fluid equilibria of hard dumbbells have been studied intensively by density-functional theory [2,3] and computer simulations [4–6]. However, for simple nonspherical molecules, effects other than size and shape can play an important role, such as dispersion forces, Coulombic, and quadrupolar interactions. This might explain the stability of the $\alpha-N_2$ crystal phase of nitrogen, which is not a stable crystal structure for hard dumbbells [4]. Still, hard dumbbells can be regarded as a reference system for simple molecules in the same way that hard spheres can serve as a reference system for monatomic fluids.

Recently, new routes to synthesize colloidal dumbbells have become available and the interest in dumbbells has been revived [7–9]. However, the size distributions of these dumbbells is relatively large and often the quantities that can be synthesized are very small. A new method has been proposed to synthesize large quantities of monodisperse colloidal dumbbells for which the aspect ratio can be tuned very easily [10]. In this method, the anisotropic particles are formed by destabilizing a dispersion of colloidal silica spheres resulting in an initial aggregation of the spheres, i.e., dumbbell formation. Subsequently, a layer of silica is grown around these cores to obtain a dumbbell of any length-to-diameter ratio $L^*=L/\sigma$, where L is the distance between the centers of the spheres and σ is the diameter of the dumbbell. By adding salt to the solvent, the dumbbell interactions can be tuned from hard to long-range repulsive interactions. Moreover, interest in colloidal dumbbells has been triggered by their potential use in photonic applications. In a photonic band-gap crystal, light of certain frequencies cannot propagate, irrespective of its direction or polarization. Photonic band-gap calculations show, however, that a complete band gap is not possible in a simple system of spherical particles, while a complete band gap can be opened by using slightly anisotropic particles [11,12]. For instance, it has been shown that dumbbells on a face-centered-cubic (fcc) lattice in which the spheres of the dumbbells form a diamond structure exhibit a complete band gap [11,12]. Unfortunately, this crystal structure is not stable in the bulk, but it does show that anisotropic particles are promising for photonic applications. The availability of this new model system of colloidal dumbbells and their potential use for photonic applications warrants a more detailed study of the phase behavior of these particles.

Previous computer simulation studies of hard dumbbells have shown the stability of at least three different solid phases. For small anisotropies and low densities, the dumbbells form a plastic crystal phase in which the particles are on an fcc lattice, but are free to rotate. At sufficiently high density, the orientationally ordered crystal phase (called CP1 in Ref. [4]) becomes stable for all anisotropies. In the ordered solid phase, the dumbbells are arranged into two-dimensional hexagonal close-packed (hcp) layers in such a way that the spheres of each dumbbell also form a hcp layer. The orientations of the dumbbells are parallel with an angle of $\arcsin(L^*/\sqrt{3})$ between the dumbbell axis and the normal of the hexagonal layers. The hexagonal layers of dumbbells are stacked in an *ABC* sequence, so that the spheres form an fcc crystal structure. At larger anisotropies, the particles can freeze into an aperiodic crystal in which not only their orientations but also the centers of mass of the dumbbells are disordered, although the spheres of each dumbbell are on a random-hexagonal-close-packed (rhcp) lattice at $L^*=1$ and at close packing. When L^* is smaller than the lattice constant, the spheres must be slightly off-lattice and then the crystal is truly aperiodic in all the coordinates. Monte Carlo simulations have shown that the aperiodic crystal is more stable than the ordered solid in a two-dimensional system of hard dimers [13–16].

The stability of an aperiodic crystal structure for a three-dimensional system of hard dumbbells has been proven by free-energy calculations and theory in Ref. [17], but only for $L^*=1$.

In the present paper, we first address the question of whether the fcc or hcp structure of the plastic crystal has the lowest free energy for hard dumbbells. The fcc and hcp structures both consist of hexagonally close-packed layers, but they differ in the way the planes are stacked. The stacking sequence for fcc is *ABC*, while it is *ABAB* for hcp. The question of which configuration is the most stable structure for hard spheres has been a long-standing issue in the literature. However, it is now well-accepted that the fcc crystal is more stable, although the free-energy difference is very small, $<10^{-3}k_BT$ per particle, with k_BT the thermal energy, k_B Boltzmann's constant, and T the temperature [18–21]. In this paper, we show that the hcp structure is more stable for hard dumbbells for a large part of the stable plastic crystal regime. Furthermore, the free-energy difference is more than an order of magnitude larger than in the case of hard spheres.

In the second part of this paper, we study the stability of an orientationally disordered aperiodic crystal structure for $L^*>0.88$. We confirm that the aperiodic crystal structure is stable for hard dumbbells and we determine the fluid-aperiodic crystal and aperiodic-periodic crystal coexistence regions using free-energy calculations. However, to the best of our knowledge, we are not aware of any atomic counterpart of the aperiodic crystal phase of hard dumbbells, or any evidence of a colloidal aperiodic crystal structure. We hope that our findings will stimulate a more detailed experimental investigation of the phase behavior of (colloidal) dumbbells.

II. MODEL

We consider a system of hard dumbbells consisting of two fused hard spheres of diameter σ with the centers separated by a distance L. We define the reduced bond length or anisotropy of the dumbbell by $L^*\equiv L/\sigma$, such that the model reduces to hard spheres for $L^*=0$ and to tangent spheres for $L^*=1$. We study the phase behavior of hard dumbbells using computer simulations for $0\leq L^*\leq 1$. We focus our attention on the plastic crystal phase for $L^*<0.4$ and the aperiodic crystal phase for $L^*>0.9$. Below we describe the simulation methods that we employ to study the plastic crystal and the aperiodic crystal structures.

III. METHODS AND RESULTS

A. Plastic crystal: hcp vs fcc

We calculate the free energy of both the fcc and the hcp plastic crystal phase by thermodynamic integration using the Einstein crystal as a reference state [22]. The Einstein integration scheme that we employ here involves the usual integration over a path through parameter space that connects the system of interest with the noninteracting Einstein crystal, without crossing a first-order phase transition. This means that the Einstein crystal must have the same symmetries as the plastic crystal phase. In particular, the dumbbells must be free to rotate, while the centers of mass are fixed to their ideal lattice positions using a harmonic spring with dimensionless spring constant λ. The potential energy function for the harmonic coupling of the particles to their ideal lattice positions reads

$$\beta U(\mathbf{r}^N,\mathbf{u}^N;\lambda)=\lambda\sum_{i=1}^{N}(\mathbf{r}_i-\mathbf{r}_{0,i})^2/\sigma^2, \tag{1}$$

where $\mathbf{r}_i$ and $\mathbf{u}_i$ denote, respectively, the center-of-mass position and orientation of dumbbell i, $\mathbf{r}_{0,i}$ is the lattice site of particle i, and $\beta=1/k_BT$. The usual thermodynamic integration path for hard spheres consists of a gradual increase of λ from 0, i.e., the system of interest, to $\lambda_{\max}$, where $\lambda_{\max}$ is sufficiently high that the system reduces to a noninteracting Einstein crystal. However, this method fails in the case of freely rotating hard dumbbells as the system will never reach the limit of a noninteracting Einstein crystal due to the rotational degrees of freedom of the dumbbells: if the lattice constant is smaller than $\sigma+L$, the dumbbells will collide while rotating even if their centers of mass are fixed at their lattice sites. We therefore combine the usual Einstein integration method with the thermodynamic integration technique that was introduced recently for hard spheres by Fortini *et al.* [23], which is based on penetrable potentials that allow us to change gradually from a noninteracting system to a system of freely rotating hard dumbbells. We changed the dumbbell-dumbbell potential energy function to

$$\beta U_{\text{soft}}(\mathbf{r}^N,\mathbf{u}^N;\gamma)=\sum_{i<j}\sum_{\eta,\mu}\beta\varphi(|\mathbf{r}_{i\eta}-\mathbf{r}_{j\mu}|,\gamma) \tag{2}$$

with

$$\beta\varphi(r,\gamma)=\begin{cases}\gamma[1-A(r/\sigma)^2], & r<\sigma,\\ 0 & \text{otherwise},\end{cases} \tag{3}$$

where $\mathbf{r}_{i\eta}$ with $\eta=\pm 1$ are the positions of the two spheres of dumbbell i, A is an adjustable parameter that is kept fixed during the simulation at a value $A=0.9$, and γ is the integration parameter. The limit $\gamma\to\infty$ reduces to the hard-core interaction, but convergence of the thermodynamic integration is already obtained for $\gamma_{\max}=200$. In Ref. [23] it was shown that in order to minimize the error and maximize the efficiency of the free-energy calculation, the potential must decrease as a function of r and must exhibit a discontinuity at r such that both the amount of overlap and the number of overlaps decrease upon increasing γ. Here, we have chosen this particular form of the potential because it can be evaluated very efficiently in a simulation. We start at a very high value of $\gamma_{\max}=200$ where the particles behave as hard dumbbells. Subsequently, we turn on the springs that couple the dumbbells to the lattice by increasing λ from 0 to $\lambda_{\max}$. We then decrease γ to 0 such that the system becomes an ideal Einstein crystal. By integrating over both paths and adding the free energy of the noninteracting Einstein crystal, one obtains the Helmholtz free energy F of a plastic crystal of hard dumbbells,

$$\beta F(N,V,T) = \beta F_{\text{Einst}}(N,V,T) - \int_0^{\lambda_{\max}} d\lambda \left\langle \frac{\partial \beta F}{\partial \lambda} \right\rangle_{\gamma_{\max}} + \int_0^{\gamma_{\max}} d\gamma \left\langle \frac{\partial \beta F}{\partial \gamma} \right\rangle_{\lambda_{\max}}, \tag{4}$$

where

$$\langle \partial \beta F/\partial \lambda \rangle = \left\langle \sum_{i=1}^{N} (\mathbf{r}_i - \mathbf{r}_{0,i})^2/\sigma^2 \right\rangle$$

and

$$\langle \partial \beta F/\partial \gamma \rangle = \langle \beta U_{\text{soft}}(\mathbf{r}^N, \mathbf{u}^N; \gamma)/\gamma \rangle.$$

The Helmholtz free energy of the noninteracting Einstein crystal plus the center-of-mass correction terms [22] reads

$$\beta F_{\text{Einst}} = -\frac{3(N-1)}{2} \ln\left[\frac{\pi}{\lambda_{\max}}\right] + N \ln\left[\frac{\Lambda_t^3}{\sigma^3}\right] + N \ln[\Lambda_r] + \ln\left[\frac{\sigma^3}{VN^{1/2}}\right], \tag{5}$$

where $\Lambda_t = (h^2/2\pi m k_B T)^{1/2}$ denotes the de Broglie wavelength and $\Lambda_r = (h^2/8\pi^2 I k_B T)^{1/2}$ with m the mass and I the moment of inertia. We determine the Helmholtz free energy F_{fcc} and F_{hcp} of the fcc and hcp plastic crystal, respectively, as a function of the reduced density ρ^* and anisotropy $0.1 \leq L^* < 0.4$. We define the dimensionless density as

$$\rho^* = \frac{d^3 N}{V}, \tag{6}$$

where $d^3/\sigma^3 = 1 + \frac{3}{2}L^* - \frac{1}{2}(L^*)^3$ is the volume of a dumbbell divided by that of a sphere with diameter σ, so d is the diameter of a sphere with the same volume as the dumbbell. The initial configurations for the plastic crystal are generated by placing the dumbbells on an fcc or hcp lattice and by picking random directions for the dumbbells until the dumbbells do not overlap anymore. For state points close to the plastic crystal-CP1 coexistence region, we use isobaric-isothermal (*NPT*) simulations to generate initial configurations. We perform simulations of 864 particles for the fcc and 900 particles for the hcp plastic crystal. We use a 20-point Gauss-Legendre integration for both the γ and λ integration.

We find that for $L^* = 0.05$ and 0.1 at low densities, the free-energy difference is very small, $< 0.001 k_B T$ per particle. As the free energies of the fcc and hcp plastic crystal are almost equal, subtracting the free energies will give rise to large errors in the free-energy differences. Moreover, we find that the result of the γ integration depends on the precise details of the numerical integration method. This dependence is small compared to the free energy of either phase, but it is a significant error relative to the free-energy *difference* between the phases. In order to circumvent this problem, we measure directly the free-energy difference in a single simulation using the so-called lattice-switch multicanonical Monte Carlo method [21]. This method has been used successfully to calculate the difference in free energies of the fcc and hcp phase for hard spheres [19–21]. Below, we discuss briefly the method and its extension to dumbbells. For a detailed description of the method, we refer the reader to Ref. [21].

The lattice-switch Monte Carlo method is based on a lattice-switch transformation that maps an fcc configuration onto an hcp configuration, and vice versa. This enables us to sample in a single simulation both crystal structures and to measure the difference in free energies by measuring the probability to find the system in one of the two phases. To this end, we express coordinate $\mathbf{r}_i$ of particle i in terms of its displacement $\Delta\mathbf{r}_i$ from its ideal lattice position $\mathbf{R}_i^{(\alpha)}$ in phase α, i.e., $\mathbf{r}_i = \mathbf{R}_i^{(\alpha)} + \Delta\mathbf{r}_i$. A lattice switch from lattice α to lattice β is then defined by $\mathbf{r}_i = \mathbf{R}_i^{(\alpha)} + \Delta\mathbf{r}_i \rightarrow \mathbf{R}_i^{(\beta)} + \Delta\mathbf{r}_i$, for particles $i = 1, \ldots, N$. In the present work, we fixed the orientations of the dumbbells during the lattice switch. The states for which we can perform the lattice switch without causing any overlaps are rare. We therefore bias the sampling to favor the gateway states, which allows us to perform the lattice switch. We define an order parameter that measures how close we are to those gateway states,

$$\mathcal{M}(\{\Delta\mathbf{r}\}) = \mathcal{M}(\{\Delta\mathbf{r}\}, \text{hcp}) - \mathcal{M}(\{\Delta\mathbf{r}\}, \text{fcc}), \tag{7}$$

where $\mathcal{M}(\{\Delta\mathbf{r}\}, \alpha)$ denotes the number of overlaps in the configuration where the particle positions are given by the set of displacements $\{\Delta\mathbf{r}\}$ in phase α. For an fcc structure, $\mathcal{M} \geq 0$, while an hcp structure corresponds to $\mathcal{M} \leq 0$. If $\mathcal{M} = 0$, there will be no overlaps in both the fcc and hcp structure, and a lattice switch will be successful. By assigning multicanonical weights $\exp[\eta(\mathcal{M})]$ to each macrostate $\mathcal{M}$, we can bias the system toward the switching states, where $\mathcal{M} = 0$.

We first measure the probability distribution $\mathcal{P}(\mathcal{M})$ of being in state $\mathcal{M}$ for an unbiased system, i.e., multicanonical weights $\eta(\mathcal{N}) = 0$. Subsequently, we use the $\mathcal{P}(\mathcal{M})$ to define the multicanonical weights in the biased sampling for the next simulation using

$$\eta(\mathcal{M}) = -\ln[\mathcal{P}(\mathcal{M})] + C_0, \tag{8}$$

where C_0 is an arbitrary constant. In this simulation, we measure the biased probability distribution correct for the bias to obtain the new estimate for $\mathcal{P}(\mathcal{M})$ and use the above expression to get the new weights. We repeat this process until the measured probability distribution in the biased simulation is essentially flat. We then use these weights in a long simulation to calculate the final $\mathcal{P}(\mathcal{M})$.

The probability $\mathcal{P}(\mathcal{M})$ can either be measured directly in a simulation by the number of times a macrostate is visited, i.e., the visited-state (VS) method, or one can measure in a simulation the bias-corrected transition probability matrix $\rho(\mathcal{M} \rightarrow \mathcal{N})$ of going from state $\mathcal{M}$ to $\mathcal{N}$ and use the "detailed balance" condition

$$\mathcal{P}(\mathcal{M})\rho(\mathcal{M} \rightarrow \mathcal{N}) = \mathcal{P}(\mathcal{N})\rho(\mathcal{N} \rightarrow \mathcal{M}) \tag{9}$$

in order to obtain $\mathcal{P}(\mathcal{M})$, i.e., the transition probability (TP) method.

We use the lattice-switch Monte Carlo method to measure directly the Helmholtz free energy in a simulation of 1728 particles. We expect the finite-size effects to be small for this

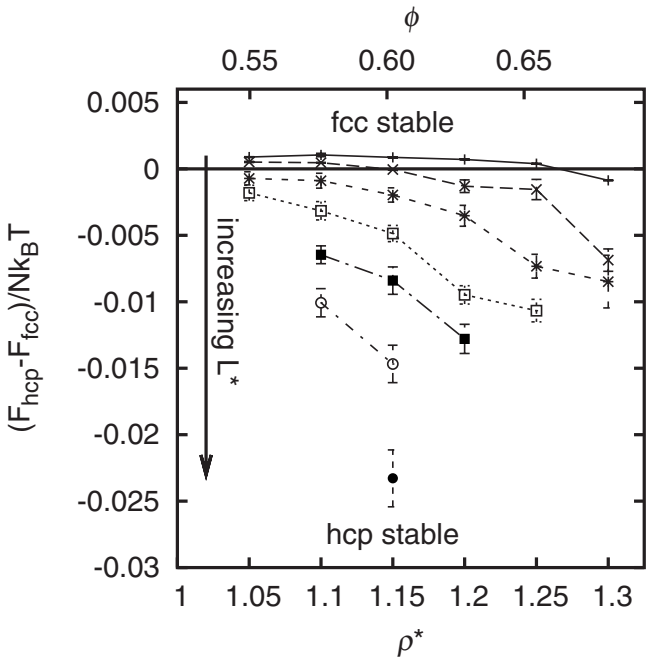

FIG. 1. The difference in the Helmholtz free energies of the hcp plastic crystal F_{hcp} and the fcc plastic crystal F_{fcc} as a function of ρ^* and $\phi=(\pi d^3/6)N/V$ for different $L^*=0.05,0.1,\ldots,0.35$ from top to bottom. The free-energy difference at $L^*=0.05$ and the one at $L^*=0.1$ with $\rho^*<1.2$ are results from the lattice-switch Monte Carlo calculations (error bars are smaller than the symbols), while all other points are obtained using the Einstein integration method.

system size. We use the transition probability method to determine the set of multicanonical weights. In Fig. 1, we show the Helmholtz free-energy difference $F_{\mathrm{hcp}}-F_{\mathrm{fcc}}$ using the Einstein crystal thermodynamic integration method and the lattice-switch Monte Carlo method as a function of ρ^* [and packing fraction $\phi\equiv(\pi d^3/6)N/V$] for varying L^*. Figure 1 clearly shows that the stability of hcp with respect to fcc increases upon increasing L^*. It is striking that even for $L^*=0.05$, hcp is more stable for sufficiently high densities, since it is well known that the fcc phase is the most stable one for hard spheres. For $L^*>0.1$, the hcp plastic phase is stable for all densities that we considered. Furthermore, the absolute value of the Helmholtz free-energy difference increases by more than an order of magnitude upon increasing L^*. The maximum value of the Helmholtz free-energy difference per particle that we find is $0.023(2)k_BT$ for $L^*=0.35$, which is more than a factor of 20 larger than the free-energy difference for hard spheres at close packing.

B. Aperiodic vs periodic crystal

We now turn our attention to the stability of the aperiodic crystal phase with respect to the periodic crystal structure. At large anisotropies and sufficiently high densities, we expect the aperiodic crystal phase to be stable.

1. Aperiodic crystal phase

In an aperiodic crystal at close packing and $L^*=1$, the individual spheres of the dumbbells are arranged on a close-packed fcc lattice, while the dumbbells, which can be considered as bonds between two sites, are chosen randomly. In the remainder of the paper, such an arrangement is referred to as a bond configuration. If there are Ω_{aper} possible bond configurations that all have the same free energy F_{conf}, the total free energy of the aperiodic crystal reads

$$\beta F = -\ln \Omega_{\mathrm{aper}} + \beta F_{\mathrm{conf}}. \tag{10}$$

Ignoring the slight variation of F_{conf} for now, we average F_{conf} over several typical aperiodic bond configurations and use this value. Furthermore, we approximate Ω_{aper} by the multiplicity at close packing and $L^*=1$. We note, however, that Ω_{aper} may depend on density and L^*, which we ignore here for simplicity.

In order to determine the multiplicity of the aperiodic crystal Ω_{aper} at close packing and $L^*=1$, we introduce a method that allows us to switch from the aperiodic crystal phase to a reference phase of which the degeneracy is known, and vice versa. By measuring the probability that the system is in either of the two phases, we can determine the multiplicity of the aperiodic phase,

$$\Omega_{\mathrm{aper}} = \mathcal{P}_{\mathrm{aper}}/\mathcal{P}_{\mathrm{ref}} \times \Omega_{\mathrm{ref}}, \tag{11}$$

where the subscript "ref" denotes the periodic reference phase.

For the reference phase, we use the so-called CP3 phase, which is the phase where all the dumbbells are arranged into two-dimensional hexagonal layers with all the particles, as in the CP1 phase, aligned in the same direction within the hexagonal layer, while the tilt angle alternates between successive layers. However, in order to form a close-packed crystal, the particles in different hexagonal layers can point in three different directions, yielding a certain degeneracy for the CP3 phase as well. The degeneracy of CP3 can be calculated by considering all 3^{N_z} possibilities for the directions of the N_z hexagonal layers, and by correcting for the number of possibilities that are identical if one takes into account the periodic boundary conditions in the z direction.

In order to measure the probability ratio as defined in Eq. (11), we first define an order parameter that enables us to distinguish the CP3 phase from the aperiodic phase. We define the parallel bond order parameter $\mathcal{N}\equiv\frac{1}{4}\Sigma_{i=1}^{2N}\Sigma_{j=1}^{6}f_{ij}$, where the first sum runs over all sites i of the lattice and the second sum runs over the six nearest neighbors j of site i within the same layer. If the dumbbell, which has a sphere on site i, is parallel to the dumbbell that has a sphere on site j, $f_{ij}=1$, otherwise $f_{ij}=0$. Since every bond is counted twice and the number of parallel bonds can change by a minimum of two, the factor 4 ensures that $\mathcal{N}$ changes by at least 1 if we change the bond configuration. For the CP3 phase, $\mathcal{N}=2N\times 6/4=3N$, since all six neighbors of all $2N$ sites are parallel in this phase.

We now introduce a MC move that allows us to generate a new configuration of bonds with a different value of $\mathcal{N}$. This bond switch move involves disconnecting and reconnecting bonds until a new configuration is found. For more technical details, we refer the reader to Appendix A. We now employ the bond switch move for a random hcp crystal

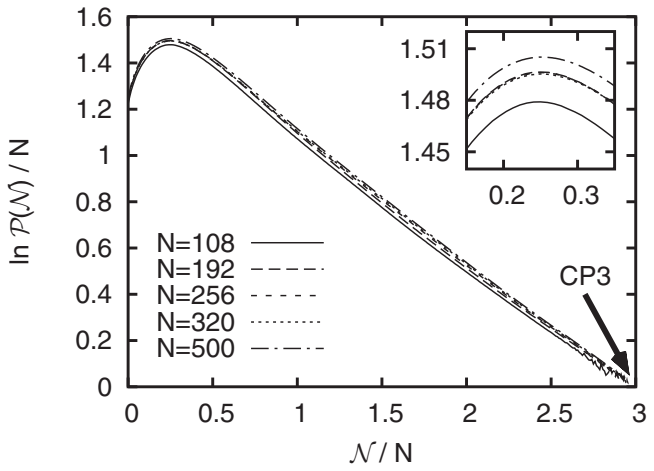

FIG. 2. The probability distribution $\ln \mathcal{P}(\mathcal{N})$ of the parallel bond order parameter $\mathcal{N}$ for systems with varying particle numbers N. The inset shows an enlarged view of the region where $\mathcal{P}(\mathcal{N})$ is maximal.

phase with $L^*=1$. We use the multicanonical Monte Carlo method to measure the probability $[\mathcal{P}(\mathcal{N})]$ of being in state $\mathcal{N}$ using weights $\eta(\mathcal{N})$, which are refined using the VS method. The probability ratio reads simply

$$\frac{\mathcal{P}_{\text{aper}}}{\mathcal{P}_{\text{CP}}3} = \frac{\sum_{\mathcal{N}<3N} \mathcal{P}(\mathcal{N})}{\mathcal{P}(\mathcal{N}=3N)}. \tag{12}$$

In Fig. 2, we plot the probability distribution $\mathcal{P}(\mathcal{N})$ of the parallel bond order parameter $\mathcal{N}$ for systems with varying particle numbers N. We note that the probability distribution $\mathcal{P}(\mathcal{N})$ has a maximum of about $\exp[1.5N]$ at $\mathcal{N}/N \simeq 0.25$. In Fig. 3, we plot the degeneracy of the aperiodic crystal phase as a function of the number of particles N. For comparison,

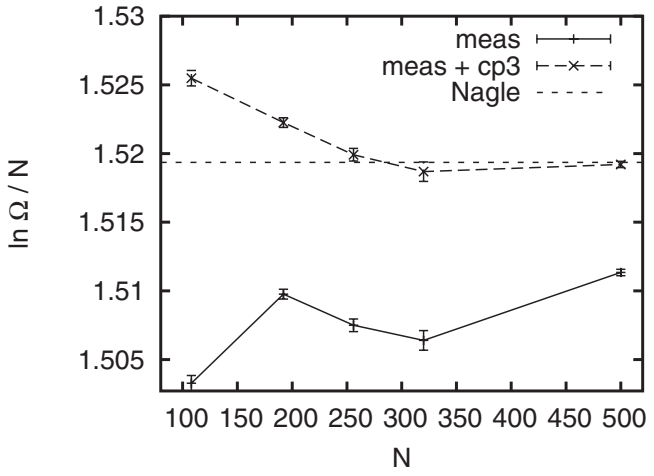

FIG. 3. The logarithm of the degeneracy of the aperiodic crystal as a function of the number of particles N. "meas" denotes the measured free-energy difference between CP3 and the aperiodic phase, in "meas+CP3" the degeneracy of CP3 is included, and "Nagle" denotes the theoretical result $\ln(4.5693) \simeq 1.519$ [24].

we also plot the theoretical result of Ref. [24], and we find good agreement for $N \geq 256$.

We determine F_{conf} at $L^*=1$ using the Einstein integration method as described above for the plastic crystal phase. However, we include an additional coupling of the orientation of dumbbell i, i.e., $\mathbf{u}_i$, to an aligning field. The potential energy function that we use to achieve both couplings reads

$$\beta U(\mathbf{r}^N,\mathbf{u}^N;\lambda) = \lambda \sum_{i=1}^{N} (\mathbf{r}_i - \mathbf{r}_{0,i})^2/\sigma^2 + \sum_{i=1}^{N} \lambda[1 - |\cos(\theta_{i0})|] + \beta U_{\text{soft}}(\mathbf{r}^N,\mathbf{u}^N;\gamma), \tag{13}$$

where θ_{i0} is the angle between $\mathbf{u}_i$ and the ideal tilt vector of particle i. The ideal tilt vectors of all particles are measured in an NPT simulation. The free energy of the hard dumbbell system $\beta F(N,V,T)$ can now be related to the known free energy of an Einstein crystal by thermodynamic integration,

$$\begin{aligned}\beta F(N,V,T) &= \beta F_{\text{Einst}}(N,V,T) - \int_0^{\lambda_{\max}} d\lambda \left\langle \sum_{i=1}^{N} (\mathbf{r}_i - \mathbf{r}_{0,i})^2/\sigma^2 \right\rangle_{\gamma_{\max}} \\ &\quad - \int_0^{\lambda_{\max}} d\lambda \left\langle \sum_{i=1}^{N} \lambda[1 - |\cos(\theta_{i0})|] \right\rangle_{\gamma_{\max}} \\ &\quad + \int_0^{\gamma_{\max}} d\gamma \, \langle \beta U_{\text{soft}}(\mathbf{r}^N,\mathbf{u}^N;\gamma)/\gamma \rangle_{\lambda_{\max}}.\end{aligned} \tag{14}$$

The Helmholtz free energy of the noninteracting Einstein crystal plus the center-of-mass correction terms [22] reads

$$\beta F_{\text{Einst}} = -\frac{3(N-1)}{2} \ln\left[\frac{\pi}{\lambda_{\max}}\right] + N \ln\left[\frac{\Lambda_t^3}{\sigma^3}\right] + N \ln[\Lambda_r] + \ln\left[\frac{\sigma^3}{VN^{1/2}}\right] - N \ln[J(\lambda_{\max})], \tag{15}$$

where

$$J(\lambda) = \int_0^1 e^{\lambda(x-1)} dx = \frac{1 - e^{-\lambda}}{\lambda}. \tag{16}$$

We perform the Einstein crystal thermodynamic integration method for an aperiodic crystal with $L^*=1$ averaging over ten different bond configurations; see Table I. The initial configurations of aperiodic crystal structures for these and all other simulations of aperiodic crystals were obtained in two steps. First, we generated ten configurations of dumbbells with $L^*=1$ at close packing, using moves similar to bond switch moves. Secondly, starting at $L^*=1$, then decreasing L^* in steps of 0.01, we measured the average configuration in an NPT simulation with $P^*=100$, which was stored to be used as an initial configuration for the simulation at the next L^* and for all further simulations of the aperiodic phase.

The Helmholtz free energy of the hard dumbbell systems for lower L^* and arbitrary density ρ^* is obtained by the following thermodynamic integrations:

TABLE I. Excess free energies, $f_{\rm exc} \equiv (F - F_{\rm id})/(Nk_BT)$, of the aperiodic and periodic phase, where $F_{\rm id}$ is the ideal gas free energy.

Phase	L^*	ρ^*	$f_{\rm exc}$
aper	1	1.15	13.887(7)
CP1	1	1.181	14.176(2)
CP1[a]	1	1.15	13.45
CP1	0.95	1.216	14.555(3)
CP1[a]	0.95	1.181	11.28
CP1	0.88	1.2283	14.172(3)
CP1[a]	0.88	1.181	10.71

[a]Calculated using thermodynamic integration (17).

$$\beta F(\rho_1^*, L^*) = \beta F(\rho_0^*, L^*) + \int_{\rho_0^*}^{\rho_1^*} d\rho \left\langle \frac{\beta P(\rho, L)}{\rho^2} \right\rangle, \quad (17)$$

$$\beta F(\rho^*, L_1^*) = \beta F(\rho^*, L_0^*) + \int_{L_0^*}^{L_1^*} dL \left\langle \frac{\partial \beta F(\rho^*, L)}{\partial L} \right\rangle. \quad (18)$$

The integrand in Eq. (17) is calculated using standard *NPT* simulations, in which we measure the density and average over five different bond configurations. Alternatively, we use bond switch moves in *NPT* simulations of $N-1$ dumbbells and two hard spheres to calculate the density; see Appendix A. In Figs. 4 and 5, we show the equation of state for five different aperiodic crystal structures at $L^*=1$ and 0.92, respectively. These were obtained in simulations without bond switch moves. We observe that the equations of state of all five aperiodic crystal structures are almost indistinguishable.

The derivative of the free energy with respect to the elongation L^* in Eq. (18) is determined using [25]

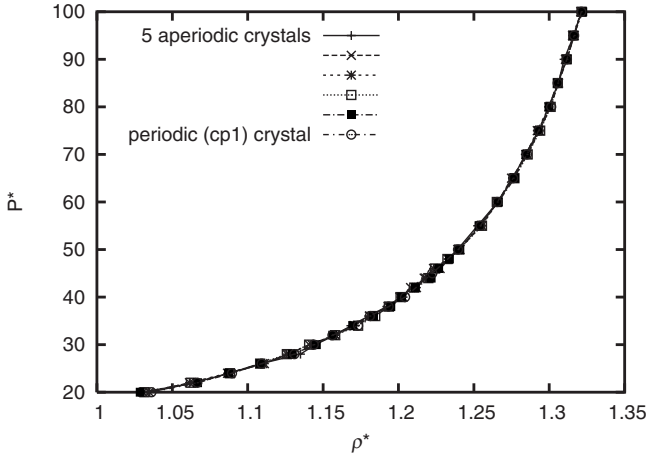

FIG. 4. The dimensionless pressure as a function of density for five different bond configurations of the aperiodic phase (aper) and for the periodic CP1 phase at $L^*=1$. The six curves are indistinguishable.

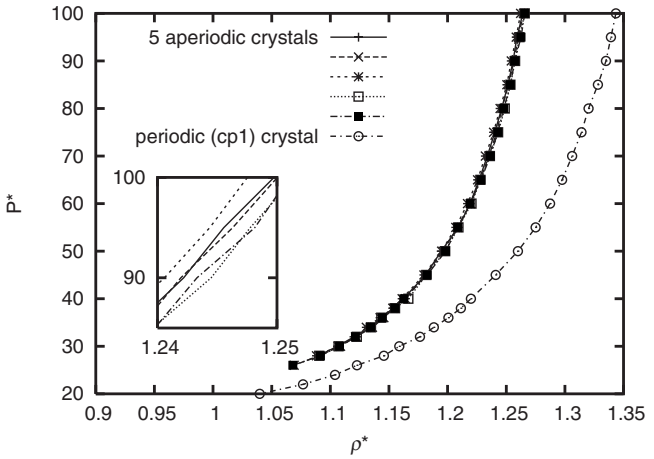

FIG. 5. The dimensionless pressure as a function of density for five different bond configurations of the aperiodic phase (aper) and for the periodic CP1 phase at $L^*=0.92$. The inset shows an enlargement to be able to distinguish the pressures of the different configurations of the aperiodic phase.

$$\left\langle \frac{\partial \beta F(\rho^*, L)}{\partial L} \right\rangle = -\frac{1}{2} \lim_{r \downarrow \sigma} \left\langle \sum_{i<j} \sum_{\eta,\mu} \delta(|\mathbf{r}_{i\eta} - \mathbf{r}_{j\mu}| - r) \times \frac{\mathbf{r}_{i\eta} - \mathbf{r}_{j\mu}}{|\mathbf{r}_{i\eta} - \mathbf{r}_{j\mu}|} \cdot (\eta \mathbf{u}_i - \mu \mathbf{u}_j) \right\rangle - \frac{3N(1-(L^*)^2)}{2+3L^*-(L^*)^2} \frac{\beta P}{\rho}, \quad (19)$$

where the latter term arises as the free-energy derivative is determined at fixed ρ^*, rather than at fixed $\rho \equiv \sigma^3 N/V$. Using a similar expression, the pressure in this term is calculated,

$$\frac{\beta P}{\rho} = 1 + \frac{1}{3N} \lim_{r \downarrow \sigma} \left\langle \sum_{i<j} \sum_{\eta,\mu} \delta(|\mathbf{r}_{i\eta} - \mathbf{r}_{j\mu}| - r) \times \frac{\mathbf{r}_{i\eta} - \mathbf{r}_{j\mu}}{|\mathbf{r}_{i\eta} - \mathbf{r}_{j\mu}|} \cdot (\mathbf{r}_i - \mathbf{r}_j) \right\rangle. \quad (20)$$

This expression is the equivalent of the virial expression for the pressure of hard spheres, $\beta P/\rho = 1 + 4\phi \lim_{r \downarrow \sigma} g(r)$, where $\phi = (\pi\sigma^3/6)N/V$ is the packing fraction. We checked that the integration of $\langle \partial \beta F/\partial L \rangle$ yields the same results within the statistical error as those obtained from the Einstein integration method. Both the virial expression for the pressure and the expression for $\langle \partial \beta F/\partial L \rangle$ require an extrapolation of r to σ. This can only be done reliably if the function to extrapolate is nearly linear, which corresponds to restricting the function to a very small interval range near σ. To get sufficient accuracy on this small interval, we need to run long simulations. For this reason, we do not use the virial expression for the pressure to obtain the equation of state; instead, we use *NPT* simulations. We perform standard *NVT* simulations to measure $\langle \partial \beta F/\partial L \rangle$ and we average over the ten initial configurations mentioned above. Alternatively, we use bond switch moves in *NVT* simulations of $N-1$ dumbbells and two hard spheres to calculate $\langle \partial \beta F/\partial L \rangle$; see Appendix B.

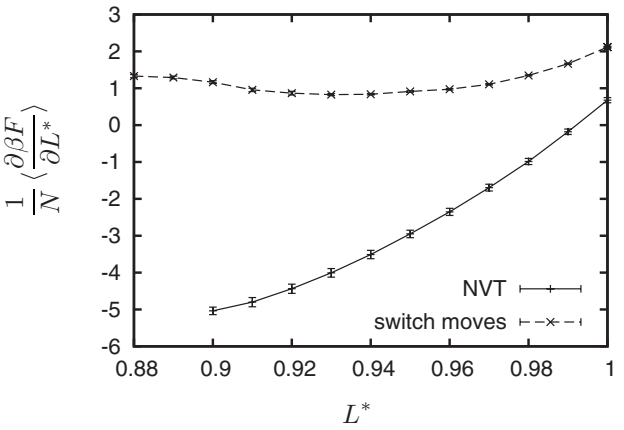

FIG. 6. The derivative of the free energy $\langle\frac{\partial\beta F}{\partial L^*}\rangle$(per dumbbell in units of k_BT) with respect to L^* at $\rho^*=1.15$ for the aperiodic phase. "*NVT*" are the results obtained from standard *NVT* simulations and averaged over 10 different bond configurations. "switch moves" denotes the results obtained from single simulations with bond switch moves.

Figure 6 shows that $\langle\partial\beta F/\partial L\rangle$ is negative and that its absolute value decreases with L^* if no bond switch moves are used. However, if bond switch moves are employed, $\langle\partial\beta F/\partial L\rangle$ is actually positive and its dependence on L is much reduced and nonmonotonic. Although $\langle\partial F/\partial L^*\rangle/N$ is rather large (in absolute value) compared to k_BT, the free-energy difference as calculated by the integral in Eq. (18) is never very large for the aperiodic phase. This is because the integration interval is no larger than the small region $(0.9\leq L\leq 1)$ where the aperiodic phase is stable.

2. Periodic crystal structure (CP1)

In order to obtain the lattice direction and lattice constant for the CP1 phase, we perform *NPT* simulation with a variable box shape [26], as the lattice direction changes as a function of density and L^* [4]. We employ these configurations in the Einstein crystal thermodynamic integration method as described in Eqs. (13)–(15) to obtain the Helmholtz free energy for varying L^*; see Table I. We perform *NPT* simulations to obtain the equation of state for varying L^*. We plot the equation of state for the CP1 phase in Fig. 4 and we find that the equation of state is indistinguishable from those of the aperiodic crystal structure for $L^*=1$. For comparison, we plot the equation of state of the CP1 phase for $L^*=0.92$ in Fig. 5. We clearly see that the pressure P^* is higher for the aperiodic crystal structure than for the CP1 phase, as the dumbbells fit less efficiently in the aperiodic crystal structure upon decreasing L^*. We obtain the Helmholtz free energy as a function of ρ^* by integrating the equation of state of CP1 for varying L^*; see Eq. (17).

3. Fluid phase

We employ the equation of state of Tildesley and Street for the fluid phase of hard dumbbells, which is known to be very accurate [1].

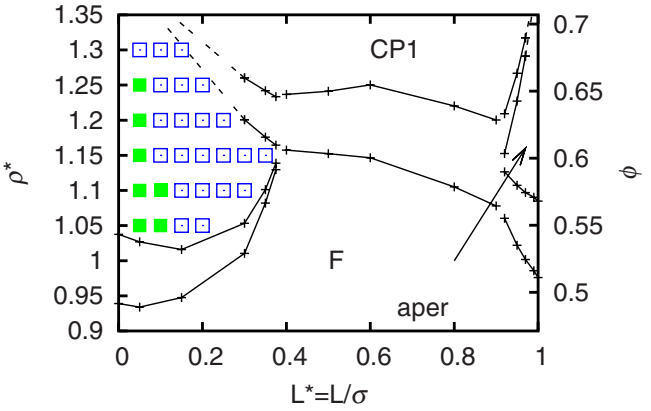

FIG. 7. (Color online) The phase diagram of hard dumbbells in the ρ^* (and packing fraction ϕ) versus $L^*=L/\sigma$ representation. *F* denotes the fluid phase and CP1 the periodic crystal. The aperiodic phase (aper) is stable only in a narrow region of the phase diagram. The stable fcc type plastic crystal is denoted by filled squares, the hcp plastic crystal phase is denoted by empty squares. The coexistence densities for $L^*<0.9$are taken from Refs. [4,5].

4. Phase diagram

We determine the fluid-plastic crystal, fluid-aperiodic crystal, and the aperiodic-CP1 crystal coexistence by employing the common tangent construction to the free-energy curves. The resulting phase diagram, together with the data from Refs. [4,5] for $L^*<0.9$, is shown in Fig. 7. We checked that the phase boundaries for the fluid-hcp plastic crystal and the hcp plastic crystal-*C*p1 coexistences hardly change compared to the results from [4,5] for the fcc plastic crystal phase. We find for $L^*>0.92$ a fluid-aperiodic crystal phase coexistence at low densities and an aperiodic-CP1 crystal phase coexistence region at higher densities. The stable region of the aperiodic crystal phase increases upon increasing $L^*\rightarrow 1$. If we measure $\langle\partial F/\partial L\rangle$ and P in simulations that include bond switch moves, the coexistence lines shift slightly, such that the aperiodic phase is stable in a larger region of the phase diagram, at the cost of the stability of the CP1 phase and, to lesser extent, the fluid phase; see Fig. 8. In Table II, the resulting coexistence data of both methods are tabulated.

If we compare our densities of the fluid-aperiodic crystal coexistence, $\rho^*_{\text{fluid}}=0.976$ and $\rho^*_{\text{aper}}=1.085$, with Ref. [17], we find a small deviation from their simulation results, $\rho^*_{\text{fluid}}=0.990$ and $\rho^*_{\text{aper}}=1.105$, while the theoretical results obtained from an extension of the Wertheim theory [27], $\rho^*_{\text{fluid}}=0.983$ and $\rho^*_{\text{aper}}=1.094$, agree slightly better with our coexistence densities. We wish to note here that it is surprising that such a simple theory predicts the fluid-solid equilibrium very accurately, as many theories fail to predict the freezing transition of molecular fluids.

IV. SUMMARY AND DISCUSSION

In this paper, we studied the phase behavior of hard dumbbells. First, we investigated whether the fcc or the hcp structure of the plastic crystal of hard dumbbells has the

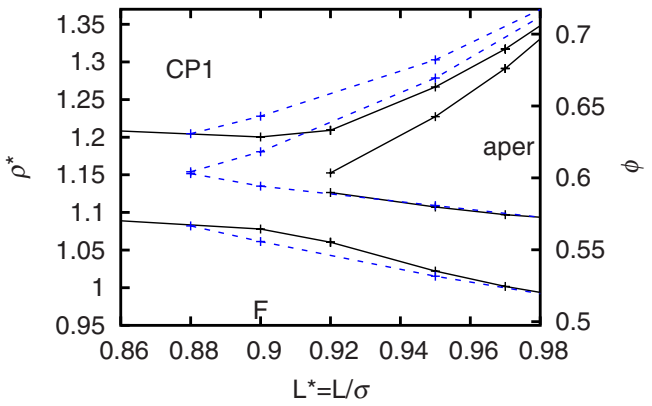

FIG. 8. (Color online) The large-L part of the phase diagram of dumbbells with (dashed line) and without bond switch moves (solid line) in ρ^* (and packing fraction ϕ) versus $L^*=L/\sigma$ representation. The lines are a guide to the eye. The stability of the aperiodic phase (aper) increases if bond switch moves are included. CP1 denotes the periodic crystal and F the fluid phase.

lowest free energy. We calculated the Helmholtz free energies of the hcp and fcc plastic crystal using the Einstein integration method and the lattice-switch multicanonical Monte Carlo method. We have shown that the hcp structure is more stable for hard dumbbells for a large part of the stable plastic crystal regime. This should be contrasted with hard spheres ($L^*=0$) for which fcc is more stable than hcp for all densities. The free-energy difference between hcp and fcc increases with L. The maximum free-energy difference is about $0.02Nk_BT$, a factor of 20 higher than that of hard spheres. The fact that this difference grows with L might be explained by the difference in available volume for a dumbbell in a fcc or hcp crystal structure. If one considers a perfect frozen fcc or hcp crystal structure with a subset of particles that are moveable, one can expand the entropy of the fcc or hcp crystal structure into the volume available for one, two, three, four, etc. moveable dumbbells in the cage formed by all the frozen particles [28]. For hard spheres, the available volume for a single sphere is identical for hcp and fcc, but the available volume for a pair of spheres is larger at close packing for the hcp phase, which would suggest that hcp is more stable for hard spheres. However, the available volume for five moveable spheres is higher for fcc than for hcp, and hence the fcc phase is more stable. As it is not possible to calculate higher-body corrections, one cannot draw any definite conclusions for hard spheres on the basis of this expansion. For dumbbells with a finite anisotropy, the free volume of a single dumbbell in the cage formed by its neighbors is different for fcc than for hcp. The difference in the available volume of a single moveable dumbbell increases with L^*, which might explain the increase in free-energy difference as L increases. However, as we did not include any higher-body corrections, we have to take this with a grain of salt. Furthermore, we conclude that including the hcp phase does not change the fluid-plastic crystal phase boundary.

In the second part of this paper, we studied the stability of an orientationally disordered aperiodic crystal structure for $L^*>0.88$. We first determined the degeneracy of the aperiodic crystal phase using a bond switch move. Subsequently, we calculated the free energy by varying methods, such as the Einstein integration method, equation-of-state integration, and integration of the derivative of the Helmholtz free energy with respect to the elongation of the dumbbells. Using the free-energy calculations, we showed that the aperiodic crystal structure is stable for hard dumbbells for $L^*\geq 0.92$ or, if bond switch moves were used, $L^*\geq 0.88$ and we have determined the fluid-aperiodic crystal and aperiodic-periodic crystal coexistence. In conclusion, we have shown the stability of two new crystal structures, i.e., the hcp plastic crystal phase and the aperiodic crystal structure, in a system of hard dumbbells. We hope that our results stimulate new experiments on colloidal dumbbells with a focus on these new structures.

APPENDIX A: BOND SWITCH MOVES AT CLOSE PACKING

A (biased) bond switch move at close packing is very similar to the configurational bias Monte Carlo (CBMC) method [22].

It consists of the following steps:

(i) *Step 1*. Choose a site of the lattice at random. This site is called the loose end and its position is labeled $\mathbf{r}(1)$. Break the bond that connects the loose end to another site at $\mathbf{r}(0)$.

(ii) *Step 2 to* $n-1$. Pick a nearest neighbor of the loose

TABLE II. Densities, pressures, and chemical potentials $\mu^*=\beta\mu-\ln(\Lambda_t^3\Lambda_r/\sigma^3)$ of the fluid-aperiodic crystal and the aperiodic crystal-CP1 coexistences at various L^*; see also Fig. 8.

Using standard MC simulations							Using bond switch moves						
L^*	phase 1	phase 2	ρ_1	ρ_2	βPd^3	μ^*	L^*	phase 1	phase 2	ρ_1	ρ_2	βPd^3	μ^*
0.92	fluid	aper	1.060	1.127	32.89	40.21	0.88	fluid	aper	1.082	1.152	35.15	41.94
0.92	aper	CP1	1.153	1.209	37.66	44.40	0.88	aper	CP1	1.154	1.205	35.62	42.34
0.95	fluid	aper	1.022	1.107	28.04	35.84	0.90	fluid	aper	1.061	1.135	32.34	39.50
0.95	aper	CP1	1.227	1.267	54.72	58.48	0.90	aper	CP1	1.181	1.228	40.37	46.43
0.97	fluid	aper	1.002	1.097	25.90	33.91	0.95	fluid	aper	1.015	1.109	27.12	34.94
0.97	aper	CP1	1.291	1.317	86.88	83.60	0.95	aper	CP1	1.279	1.303	72.30	72.14
1.00	fluid	aper	0.976	1.085	23.60	31.85	1.00	fluid	aper	0.977	1.083	23.67	31.92

FIG. 9. An example of the bond switch move on a hexagonal lattice. The dumbbells are denoted by thick lines, the loose spheres by circles: $\mathbf{r}(0)$ is shown by the open circle and the loose end, $\mathbf{r}(1)$ is shown by the filled symbol. The bond configuration is depicted at the instant just after the bond indicated by a dashed line has been disconnected and before a new bond is chosen.

end with probability $\mathcal{P}_i$. We use $\mathcal{P}_i=\exp[-\beta u_i]/w_i$, where $u_i=\lambda_b|\mathbf{r}_i-\mathbf{r}(0)|^2$, and $w_i=\Sigma_k\exp(-\beta u_k)$; the sum is over all the neighbors of the loose end and $\mathbf{r}_i$ is the position of neighbor i. We disconnect the bond that paired this neighbor i with another site at $\mathbf{r}(1)$, which becomes the new loose end. In this way, the loose end will make a trajectory throughout the system.

(iii) *Step n.* After a certain number of steps, one of the neighbors of the loose end is site $\mathbf{r}(0)$. If this site is selected we connect the loose end to $\mathbf{r}(0)$. There are no loose ends anymore in the system and the bond switch move is complete. The length of the trajectory is determined by λ_b. An example of the entire bond switch move on a hexagonal lattice is depicted in Fig. 9. We note that in our simulations bond switch moves are performed in three dimensions.

The bond switch move satisfies detailed balance as the probability to generate the new bond configuration starting with the old bond configuration equals the probability of generating the old configuration from the new configuration, since both probabilities are equal to products of the same factors P_i, the only difference being the order in which the factors occur.

APPENDIX B: OFF-LATTICE BOND SWITCH MOVES

For densities lower than close packing or if $L^*<1$, not all bond configurations are equally probable. However, if we are able to construct a bond switch move that visits configurations with a Boltzmann probability, i.e., that obeys detailed balance, we can take this into account. Two problems arise when one applies the bond switch move as it was defined in the last section to lower ρ^* and L^*. First of all, the connection and reconnection step needs to be adjusted, as spheres must be moved to detach from one dumbbell and attach to another. Suppose that i is a single sphere at $\mathbf{r}_i$ and j is a dumbbell with direction vector $\mathbf{u}_j$ and center-of-mass position $\mathbf{r}_j$ and that we wish to connect sphere $\eta=\pm 1$ of dumbbell j to sphere i, turning particle i into a dumbbell with direction vector $\mathbf{u}_i'$ and center-of-mass position $\mathbf{r}_i'$ and particle j into a sphere at $\mathbf{r}_j'$. The way to do this is

$$\mathbf{u}_i' = (\mathbf{r}_i - \mathbf{r}_{j\eta})/a,$$

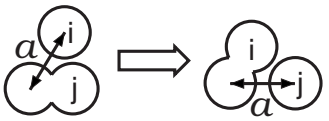

FIG. 10. A typical bond switch move for a non-close-packed structure: particles are not positioned on a lattice.

$$\mathbf{r}_i' = \mathbf{r}_{j\eta} + \frac{L}{2}\mathbf{u}_i',$$

$$\mathbf{r}_j' = \mathbf{r}_{j\eta} - a\,\eta\mathbf{u}_j, \tag{B1}$$

where $a=|\mathbf{r}_i-\mathbf{r}_{j\eta}|$; see Fig. 10. Note that the position of sphere η of the dumbbell is fixed during the move. Still, the first step of the bond switch move, disconnecting a dumbbell, will involve making an arbitrary choice for a, and for the last step, connecting two spheres, we must choose the acceptance probability of a certain value for a. The second problem is that, although the spheres are now moved to connect and disconnect a dumbbell, the bond switch move will still fail due to overlaps with the particles that are not directly involved in the bond switch move. One can resolve this problem by combining the bond switch moves with displacement moves of the particles. However, in this case one has to make sure that each step in the bond switch move preserves detailed balance, while in Appendix A only the entire bond switch move preserves detailed balance. To this end, we accept the generated move with a probability of $w(f)/w(r)$, where $w(f)$ is the weight w_i as occurring in a step in the bond switch move and $w(r)$ is the weight of the reverse move.

In this case, the system consists of $N-1$ dumbbells and two spheres during one part of the simulation and of N dumbbells during the other part. As a result, since the bond switch moves will consist of varying the numbers of steps, the sampling, which can only occur when the system consists of only dumbbells, is biased. We decided, therefore, to use a system of $N-1$ dumbbells and two spheres during the entire simulation. An additional advantage is that we do not have to bias the system anymore ($\lambda_b=0$), since the trajectory of the loose end throughout the system does not have to be closed. The results of these simulations will be nearly equal to the results of simulations of N dumbbells provided that N is large enough and that the definitions of $\partial F/\partial L$ and ρ^* are adjusted: $\rho^*\equiv[(N-1)d^3+2\sigma^3]/V$, and we approximate $\partial F/\partial L$ of N dumbbells to $N/(N-1)$ times $\partial F/\partial L$, as measured in our system of $N-1$ dumbbells and two spheres. In our simulations, we used $N=864$, and we checked that $\partial F/\partial L$ and ρ^* measured in a simulation of $N-1$ dumbbells and two spheres *without* bond switch moves were nearly equal to the results of a simulations with N dumbbells, with a difference of the order of $1/N$.

[1] T. D. Tildesley and W. B. Street, Mol. Phys. **41**, 85 (1980).
[2] S. J. Smithline, S. W. Rick, and A. D. J. Haymet, J. Chem. Phys. **88**, 2004 (1988).
[3] J. D. McCoy, S. Singer, and D. Chandler, J. Chem. Phys. **87**, 4853 (1987).
[4] C. Vega, E. P. A. Paras, and P. A. Monson, J. Chem. Phys. **96**, 9060 (1992).
[5] C. Vega, E. P. A. Paras, and P. A. Monson, J. Chem. Phys. **97**, 8543 (1992).
[6] C. Vega and P. A. Monson, J. Chem. Phys. **107**, 2696 (1997).
[7] V. N. Manoharan, M. T. Elsesser, and D. J. Pine, Science **301**, 483 (2003).
[8] G. R. Yi, V. N. Manoharan, E. Michel, M. T. Elsesser, S. M. Yang, and D. J. Pine, Adv. Mater. (Weinheim, Ger.) **16**, 1204 (2004).
[9] C. M. Liddell and C. J. Summers, Adv. Mater. (Weinheim, Ger.) **15**, 1715 (2003).
[10] P. M. Johnson, C. M. van Kats, and A. van Blaaderen, Langmuir **21**, 11510 (2005).
[11] Y. Xia, B. Gates, and Z. Li, Adv. Mater. (Weinheim, Ger.) **13**, 409 (2001).
[12] Z.-Y. Li, J. Wang, and B.-Y. Gu, Phys. Rev. B **58**, 3721 (1998).
[13] A. C. Branka and K. W. Wojciechowski, Mol. Phys. **56**, 1149 (1985).
[14] K. W. Wojciechowski, Phys. Lett. A **122**, 377 (1987).
[15] K. W. Wojciechowski, D. Frenkel, and A. C. Branka, Phys. Rev. Lett. **66**, 3168 (1991).
[16] K. W. Wojciechowski, Phys. Rev. B **46**, 26 (1992).
[17] C. Vega and L. G. MacDowell, J. Chem. Phys. **114**, 10411 (2001).
[18] P. G. Bolhuis, D. Frenkel, S.-C. Mau, and D. A. Huse, Nature **388**, 235 (1997).
[19] S.-C. Mau and D. A. Huse, Phys. Rev. E **59**, 4396 (1999).
[20] A. D. Bruce, N. B. Wilding, and G. J. Ackland, Phys. Rev. Lett. **79**, 3002 (1997).
[21] A. D. Bruce, A. N. Jackson, G. J. Ackland, and N. B. Wilding, Phys. Rev. E **61**, 906 (2000).
[22] D. Frenkel and B. Smit, *Understanding Molecular Simulation* (Academic, San Diego, 2002).
[23] A. Fortini, M. Dijkstra, M. Schmidt, and P. P. F. Wessels, Phys. Rev. E **71**, 051403 (2005).
[24] J. F. Nagle, Phys. Rev. **152**, 190 (1966).
[25] S. J. Singer and R. Mumaugh, J. Chem. Phys. **93**, 1278 (1990).
[26] M. Parrinello and A. Rahman, Phys. Rev. Lett. **45**, 1196 (1980).
[27] C. Vega, L. G. MacDowell, C. McBride, F. J. Blas, A. Galindo, and E. Sanz, J. Mol. Liq. **113**, 37 (2004).
[28] C. Radin and L. Sadun, Phys. Rev. Lett. **94**, 015502 (2005); H. Koch, C. Radin, and L. Sadun, Phys. Rev. E **72**, 016708 (2005).